nature communications

Article

https://doi.org/10.1038/s41467-025-60029-4

Structural basis for the human SENP5's SUMO isoform discrimination

Received: 27 September 2024

Accepted: 13 May 2025

Published online: 22 May 2025

Check for updates

Lucía Sánchez-Alba[1,5], Li Ying[1,4,5], Matthew D. Maletic[2], Anna De Bolòs[3], Helena Borràs-Gas[1], Bing Liu[1], Nathalia Varejão[1], Virginia Amador[3], Monique P. C. Mulder[2] & David Reverter[1]

Post-translational SUMO modification is a widespread mechanism for regulating protein function within cells. In humans, SUMO-conjugated proteins are partially regulated by the deconjugating activity of six SENP family members. The proteolytic activity of these enzymes resides within a conserved catalytic domain that exhibits specificity for the two primary SUMO isoforms: SUMO1 and SUMO2/3. SENP5, along with SENP3, are nucleolar proteins involved in ribosome biogenesis and preferentially target SUMO2/3 isoforms. Here, we present the crystal structures of human SENP5 in complex with both SUMO1 and SUMO2 isoforms. These structures reveal a minimal complex interface and elucidate the molecular basis for SENP5's preference for the SUMO2 isoform. This preference can be attributed to a basic patch surrounding SENP5 Arg624 at the interface. Swapping mutagenesis and structural analysis demonstrate that Arg624 is favorably oriented to interact with Asp63 in SUMO2/3, while its interaction with the equivalent Glu67 in SUMO1 is less favorable. These results suggest that subtle structural differences within SUMO isoforms can significantly influence their deconjugation by SENP enzymes, opening new avenues for exploring the regulation of SUMOylation in various cellular processes and for developing therapeutic agents targeting SUMOylation pathways.

SUMOylation is a post-translational modification wherein the Small Ubiquitin-like Modifier (SUMO) is covalently attached to lysine residues of target proteins. Like ubiquitin, SUMO is conjugated via its C-terminal tail through a multi-step enzymatic cascade involving E1 activation, E2 conjugation, and E3 ligation[1]. In humans, SUMOylation plays a pivotal role in diverse cellular processes, including DNA replication, nuclear transport, and DNA damage response[2–4]. SUMOylation typically modulates protein-protein interactions by binding to specific SUMO interaction motifs (SIMs)[5–7]. This modification can be reversed by deSUMOylating proteases that cleave the isopeptidic bond between SUMO and the target lysine[8–11]. SUMO is a ubiquitous modification found across eukaryotes. While humans encode four SUMO isoforms (SUMO1, SUMO2, SUMO3, and SUMO4), yeast and invertebrates have only one (Smt3), and plants have multiple[12,13]. Notably, SUMO2 and SUMO3 share a high degree of sequence similarity (97%, collectively referred to as SUMO2/3 after maturation), while SUMO1 exhibits lower similarity (47%). Interestingly, the inability of SUMO4 to be processed prevents it from forming SUMO conjugates[14].

The SENP/ULP protease family constitute the major group of deSUMOylating enzymes within human cells[8,9,15–17]. They are composed by long unstructured regions followed by a conserved catalytic domain that belongs to the CE-clan of cysteine proteases, containing

[1]Institut de Biotecnologia i de Biomedicina (IBB) and Dept. de Bioquímica i Biologia Molecular, Universitat Autònoma de Barcelona, Bellaterra, Spain. [2]Department of Cell and Chemical Biology, Leiden University Medical Center (LUMC), Leiden, The Netherlands. [3]Institut de Investigacions Biomèdiques Agustí Pi i Sunyer (IDIBABS), Barcelona, Spain. [4]Present address: Qingdao University, Qingdao, China. [5]These authors contributed equally: Lucía Sánchez-Alba, Li Ying. e-mail: david.reverter@uab.cat

the characteristic active site catalytic triad (His-Asp-Cys)[18]. Similar to ULP1, the founding member discovered in *Saccharomyces cerevisiae*[19,20], the SENP/ULP family in humans is constituted by six members that can be divided into three subfamilies based on phylogenesis and sequence homology: SENP1 and SENP2; SENP3 and SENP5; and SENP6 and SENP7[9]. However, in the recent years, two novel classes of SUMO proteases have been discovered in human cells non-related to the SENP/ULP family: the deSUMOylating peptidase 1 and 2 (DESI1 and DESI2)[21]; and the deubiquitinating enzyme USPL1, which is active for SUMO[22,23]. The SENP/ULP family members are responsible of a dual proteolytic function: processing of SUMO precursors, by cleaving off the α-peptide bond in the C-terminus of SUMO precursors (preSUMO1, preSUMO2, and preSUMO3) to expose the diglycine motif (mature SUMO); and the deconjugating activity of SUMO targets, by cleaving off the isopeptide bond between SUMO and the lysine residue of substrates[24–27]. Whereas all six members of the SENP/ULP family possess isopeptide or deconjugating activity, only the SENP1 and SENP2 subfamily are able to efficiently process the immature SUMO precursors, displaying different activities depending on the type of SUMO isoforms[26,28–30].

Substrate specificity in the SENP/ULP family is mostly regulated by localization of the different members within the cell, which is mostly determined by the unstructured regions outside the conserved catalytic domain[8,9]. In some cases, alternative splicing or post-translational modification contribute to the spatial control of the deconjugation activity[24,31–34]. For example, SENP1 and SENP2 are enriched at the nuclear pore complex and in the PML nuclear bodies during the interphase, but they accumulate at the kinetochore during mitosis[27,35–37]. SENP3 and SENP5 are mostly compartmentalized within the granular component of the nucleolus, although it can also be found at the mitochondria[38–42]. SENP6 and SENP7 are mainly located at the nucleoplasm, where they interact with chromatin regulating gene expression[25,43]. Alternatively, short splicing variants of SENP2, SENP5, and SENP7 have also been found at the cytoplasm[35,44–46].

Regarding SENP3 and SENP5 known functions, knockdown of SENP5 inhibits cell proliferation, having important defects in nuclear morphology and in cell division[47,48]. The unstructured N-terminal region of SENP5 has a major role in the restriction of SUMO deconjugation activity to the nucleolus[47], where together with SENP3, have been involved in ribosome and pre-rRNA biogenesis processes[49,50]. SENP3 and SENP5 were initially found to directly interact with B23/nucleophosmin[40]. More recently, a proteomics analysis have identified different subsets of SUMOylated trans-acting factors involved in ribosome biogenesis controlled by either SENP3 or SENP5[50]. Their data suggest that SENP5 predominantly participates in the 40S particle assembly, whereas SENP3 is connected to both 40S and 60S maturation steps[50]. SENP5 has also been involved in the regulation of the mitochondrial fission during mitosis by regulating the activity of the GTPase Drp1[41,42]. A short splicing variant of SENP5 lacking the catalytic domain has been shown to competitively regulate the SUMO conjugation of Drp1[46]. Recently, SENP5 and SENP3 have also been reported to regulate the SUMOylation levels of Aurora A kinase and thus control its activity during mitosis[51].

The structural and functional characterization of SENP/ULP family members has revealed that their specificity towards SUMO isoforms (SUMO1 vs. SUMO2/3) is primarily determined by their conserved catalytic domains[25,28–30,52–54]. These domains exhibit distinct binding affinities for each SUMO isoform. Within the three SENP subfamilies, only SENP1 and SENP2 demonstrate efficient deconjugation of both SUMO1 and SUMO2/3 isoforms[28–30]. SENP6 and SENP7 possess a unique loop insertion sequence within their catalytic domains, which expands the protein-protein contact interface and confers specific activity towards SUMO2/3 conjugates[25,52–54]. Interestingly, the SENP3 and SENP5 subfamily also exhibits a preference for deconjugating SUMO2/3 over SUMO1 in vitro, despite lacking the loop insertion characteristic of SENP7[38,40,55].

Here, we present the crystal structures of SENP5 in complex with SUMO1, SUMO1 E67D mutant, and SUMO2 isoforms at resolutions of 2.1, 1.7, and 2.3 Å, respectively. The SENP5 complex interface is notably compact, representing the smallest among known SENP/ULP member complex structures. Intriguingly, a specific basic patch surrounding Arg624 in SENP5 appears to be crucial for its preference for the SUMO2 isoform, forming a favorable ion pair as evidenced by the structure of a complex with an engineered SUMO1 E67D mutant. Our findings hold potential for the development of more selective inhibitors and probes targeting individual members of the human SENP family, such as SENP5, which play essential roles in various cellular processes.

Results

SENP5 prefers SUMO2 deconjugation

The full-length sequence of human SENP5 comprises 755 residues, and based on sequence alignments with SENP/ULP family members and on AlphaFold-2 prediction, the structure of SENP5 is composed by a N-terminal unstructured region followed by the canonical catalytic domain (Supplementary Fig. 1). Several constructs of the SENP5 catalytic domain with different N-terminal truncations have been analyzed by recombinant expression, including a construct with a 3-helix bundle domain predicted by AlphaFold-2 located N-terminal to the catalytic domain (from residue 493 to 755), which might participate in substrate binding (Supplementary Fig. 2). However, only the shortest SENP5 catalytic domain construct (from residue 568 to 755), yielded soluble protein in *Escherichia coli* and ultimately SUMO proteolytic activity in in vitro assays. This shorter SENP5 construct lacks some N-terminal secondary structure elements present in the catalytic domain of other members of the human SENP family, like a N-terminal α-helix and a short β-structure. These elements are relevant for SUMO binding in other family members, such as SENP1, SENP2, and SENP7, in the latter playing a major role in the SUMO2 isoform specificity[28–30,52].

In vitro activity assays using the catalytic domain of SENP5 (named $SENP5_{CD}$ from now on) revealed limited proteolytic processing of the three SUMO isoform precursors. Only at high $SENP5_{CD}$ concentrations (150 nM) processing activity is observed for preSUMO2, while preSUMO1 and preSUMO3 remain largely unprocessed (Supplementary Fig. 3). In contrast, $SENP5_{CD}$ exhibited robust isopeptidase activity toward SUMO2/3-conjugated substrates, evidenced when comparing time course reactions with model substrates RanGAP1-SUMO1 and RanGAP1-SUMO2/3, or with SUMO1 and SUMO2-AMC substrates at 5 nM or 50 nM $SENP5_{CD}$ concentrations respectively (Fig. 1a, b). Similar isopeptidase activity is observed for a diSUMO2 substrate, indicating its potential to process SUMO2 chains (Supplementary Fig. 3). Therefore, as reported before[40,55], our in vitro assays confirm the preference for SUMO2/3 over SUMO1, with significantly slower reaction rates for SUMO1. This proteolytic behavior aligns with the SENP6 and SENP7 subfamily but diverges from the SENP1 and SENP2 subfamily, which are active toward both SUMO1 and SUMO2/3 isoforms in deconjugation reactions[25,28–30,52].

To compare SENP5's deconjugation activities between SUMO1 and SUMO2/3, we conducted a competitive in vitro fluorogenic kinetic assay (Fig. 1c). By measuring the decay of $SENP5_{CD}$ activity against SUMO2-Rhodamine upon incubation with increasing amounts of RanGAP1-SUMO2/3 or RanGAP1-SUMO1 substrates, we found that only RanGAP1-SUMO2/3 effectively competed with the fluorescent substrate (Fig. 1c). This competition resulted in an IC_{50} (half maximal inhibitory concentration) of approximately 3.7 μM. In contrast, RanGAP1-SUMO1 showed no competition with SUMO2-Rho deconjugation up to 30 μM concentration. These results further confirm SENP5's significant preference for SUMO2/3 over SUMO1 in our in vitro assays.

https://doi.org/10.1038/s41467-025-60029-4

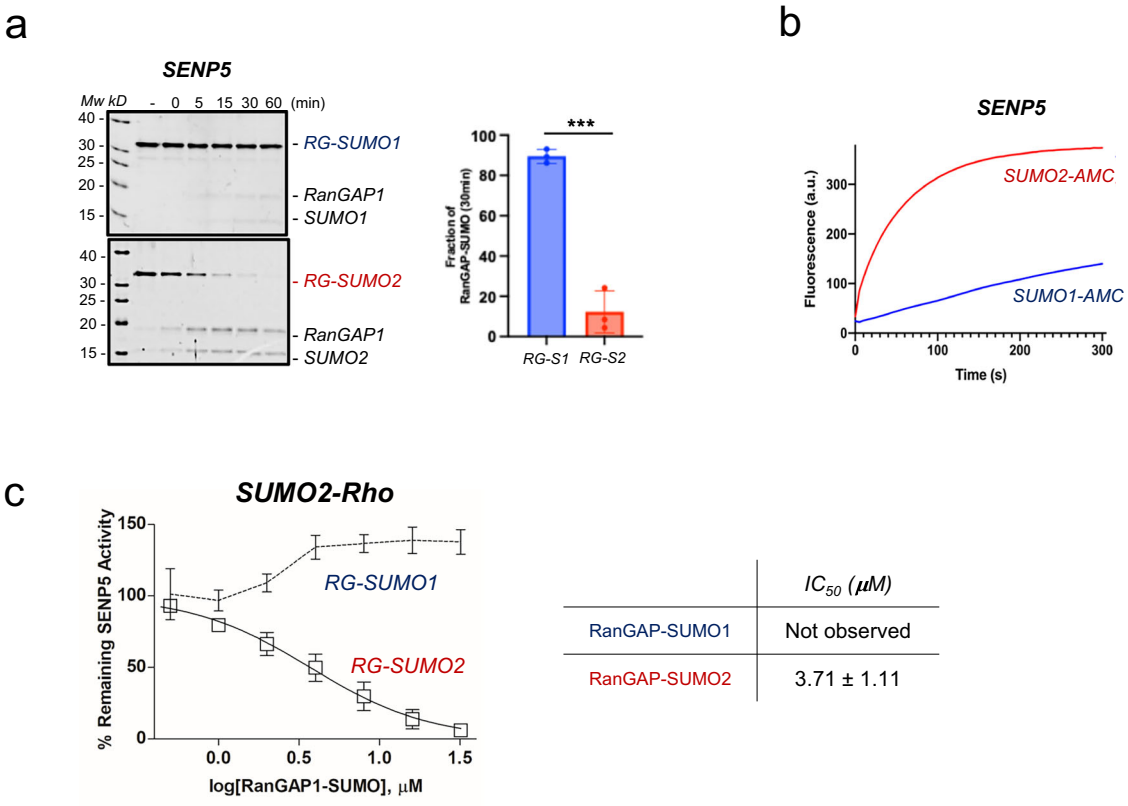

	IC_{50} (μM)
RanGAP-SUMO1	Not observed
RanGAP-SUMO2	3.71 ± 1.11

Fig. 1 | SUMO2 isoform preference of SENP5$_{CD}$ catalytic domain. a SDS-PAGE of the endpoint assays of SENP5 using RanGAP1-SUMO1 and RanGAP1-SUMO2 substrates. (*Right*) Plot of the fraction of the RanGAP1-SUMO2 substrate after 30 min reaction. Data values represent the mean ± SEM, $n = 3$ technical replicates. Significance was measured by a two-tailed unpaired *t* test relative to wild-type. All data were analyzed with a 95% confidence interval. $^{*}P \le 0.05$, $^{**}P \le 0.01$, $^{***}P \le 0.001$, $^{****}P \le 0.0001$. Exact *P* value: 0.0003. **b** Plot of the proteolytic cleavage of SUMO1-AMC and SUMO2-AMC to test the activity of SENP5. SUMO2-AMC was incubated with SENP5, and released AMC was identified by fluorescence. **c** Plot of a competition assay by measuring the interference of the SENP5 activity for SUMO2-Rhodamine substrate by competition with either RanGAP1-SUMO1 and RanGAP1-SUMO2 at different concentrations. (*Right*) Inhibitory constant values for RanGAP1-SUMO1 and RanGAP-SUMO2 substrates on the SENP5 activity on SUMO2-Rho. Data values represent the mean ± SEM, $n = 3$ technical replicates. Source data are provided as a Source Data file.

Crystal structure of the human SENP5$_{CD}$ in complex with SUMO1 and SUMO2

To elucidate the determinants of SENP5's preference for SUMO2, we engineered SUMO1 and SUMO2 with a propargylated C-terminal group (SUMO-PA). This modification allowed for covalent crosslinking of the SUMO C-terminus to the active site cysteine (Cys713) of SENP5$_{CD}$, facilitating complex crystallization. SUMO1-PA was prepared using a synthetic peptide approach[56], while SUMO2-PA was synthesized via an intein-based fusion protocol followed by propargylamine modification[57,58].

SENP5$_{CD}$ complexes with SUMO1-PA and SUMO2-PA were formed via covalent crosslinking between the SUMO C-terminal alkyne group and the SENP5$_{CD}$ active site cysteine. After cationic exchange purification, both complexes were concentrated and prepared for crystallization experiments. Diffraction quality crystals were obtained in a buffer of 2.1 M DL-Malic acid pH 7.0 for SUMO1 complex and 0.1 M HEPES 7.0, 15% PEG 20,000 for SUMO2 complex. The SENP5$_{CD}$-SUMO2 crystals belonged to $P2_12_12_1$ space group and diffracted up to 2.36 Å resolution, whereas the SENP5$_{CD}$-SUMO1 crystals belonged to $P6_522$ space group and diffracted up to 2.18 Å resolution (Table 1). Electron density maps for both complexes revealed a continuous SENP5$_{CD}$ chain from Met568 to Asp756 and confirmed the covalent bond between SUMO Gly93 and SENP5$_{CD}$ Cys713, validating the specific reaction between SENP5$_{CD}$ and the SUMO-PA activity-based probes (Fig. 2).

The SENP5 catalytic domain adopts the canonical fold characteristic of the SENP/ULP family, albeit lacking certain N-terminal secondary structure elements found in other family members (Fig. 2d). Comparison of the bound and unbound SENP5 structures (AlphaFold-2 model) revealed minimal structural rearrangements upon SUMO-PA binding (rmsd values of 0.71 Å over 190 aligned residues). Structural overlapping shows that the active site catalytic triad might already be well arranged in the absence of SUMO substrate, as compared with the AlphaFold-2 structure of the unbound SENP5$_{CD}$ (Supplementary Fig. 2). The SENP5$_{CD}$-SUMO2 interface is smaller than those observed in other SENP/ULP family members. PDBePISA[59] analysis revealed an interface area of 833 Å^2 for SENP5$_{CD}$-SUMO2, compared to 982 Å^2 and 1170 Å^2 for SENP7$_{CD}$ (PDB ID 7R2E)[52] and SENP2$_{CD}$ (PDB ID 2IO0)[29], respectively (Supplementary Fig. 4).

Structural comparison indicates a closer evolutionary relationship between SENP5$_{CD}$ and the SENP1/SENP2 subgroup than the SENP6/SENP7 subgroup, as reflected by rmsd values of 1.22 Å over 175 aligned residues (with a 37% sequence identity with SENP2) and 1.77 Å over 167 aligned residues (with a 27% sequence identity with SENP7). Despite lacking the Loop1 insertion characteristic of SENP7, which is associated with SUMO2/3 specificity, SENP5$_{CD}$ exhibits a clear preference for SUMO2/3 over SUMO1. This suggests that distinct structural determinants within the SENP5$_{CD}$ interface may underlie its stronger deconjugation activity toward SUMO2/3 isoforms.

Structural comparison of SUMO1 and SUMO2 bound to SENP5$_{CD}$ revealed minimal differences in the docking interface (Fig. 2c). However, to understand the underlying reasons for SENP5's lower isopeptidase activity toward SUMO1, a detailed analysis of specific interface contacts is necessary. While most contacts are conserved

Table 1 | Crystallographic statistics of SENP5-SUMO2, SENP5-SUMO1, and SENP5-SUMO1 E67D crystal structures

	SENP5-SUMO2	*SENP5-SUMO1*	*SENP5-SUMO1$_{E67D}$*
Data collection			
Space group	$P2_12_12_1$	$P6_522$	$P6_522$
Unit cell parameters (Å)	66.16, 87.90, 116.7	91.06, 91.06, 146.5	90.35, 90.35, 151.9
Wavelength (nm)	0.9792	0.9791	0.9791
Resolution range (Å)	48.61–2.36	78.86–2.18	69.56–1.73
R_{merge}	0.12 (1.30)*	0.14 (0.72)*	0.09 (1.42)*
R_{pim}	0.05 (0.57)*	0.04 (0.41)*	0. 03 (1.20)*
(I/σ(I))	10.8 (1.4)*	9.9 (1.5)*	11.3 (1.2)*
Completeness (%)	90.1 (49.1)*	94.2 (60.1)*	89.9 (25.0)*
Multiplicity	6.5 (6.0)*	12.3 (3.7)*	12.7 (1.1)*
CC (1/2)	0.99 (0.54)*	0.99 (0.62)*	0.99 (0.51)*
Structure refinement			
Resolution range (Å)	48.60–2.45	78.86–2.18	69.55–1.90
No. of unique reflections	23088	14291	27515
R_{work}/R_{free} (%)	19.85/26.8	19.42/25.21	21.30/25.95
No. of atoms			
Protein	4399	2197	2193
Water molecules	0	63	33
Overall B factors (Å^2)	59.3	41.5	61.4
Rms deviations			
Bonds (Å)	0.009	0.003	0.012
Angles (°)	1.030	0.579	1.190
Ramachandran favored (%)	96.76	98.08	98.46
Ramachandran allowed (%)	2.67	1.92	1.54
Ramachandran outliers (%)	0.57	0.0	0.0
PDB codes	***9GNN***	***9GNV***	***9GNX***

*Values within parenthesis are for the highest-resolution shell.

between SUMO1 and SUMO2, including key SENP/ULP family interface residues like Asp585, Phe609, and Trp625, a basic patch in the SENP5$_{CD}$ interface, consisting of Arg624 and Lys627, adopts different rotamer orientations (Fig. 2e). This patch participates in an electrostatic interaction only in the SUMO2 complex structure and resulted crucial for SENP5's SUMO2 isopeptidase activity.

SENP5$_{CD}$ interface with SUMO1 and SUMO2

The C-terminal tails of SUMO1 and SUMO2 are buried within a SENP5$_{CD}$ cleft containing the catalytic triad, which cleaves the isopeptide bond following the C-terminal diGly motif (Figs. 2 and 3a). The geometry and contacts of the C-terminal tail in both complexes are similar to those observed in other SENP/ULP family members (Fig. 3b). The interface is primarily formed by a mainchain hydrogen bond network between the SUMO C-terminal tail (Q/E89-Q90-T91-G92-G93) and SENP5$_{CD}$ mainchain residues, along with interactions involving His642 (asparagine in SENP6 and 7) and the C-terminal SUMO diGly motif sandwiched between Trp582 (phenylalanine in SENP6 and 7) and Trp647. These C-terminal contacts are basically conserved in SENP2 and SENP7 interfaces with SUMO2 (PDB IDs 7R2E and 2IO0)[29,52] (Fig. 3b).

SENP5's preference for SUMO2 likely stems from interactions within the extensive interface between its catalytic domain and the SUMO globular domain. Highly conserved residues across the SENP/ULP family, including Asp585 (electrostatic with Arg59), Phe609 (stacking with Phe87), and Trp625 (contacting Gly64) (SENP5 and SUMO2 nomenclature), are crucial for both SUMO binding and catalytic activity (Fig. 3c). Interestingly, SENP8/NEDP1, the only SENP family member specific for Nedd8, deviates from this pattern with glutamate and proline substitutions for the conserved phenylalanine and tryptophan (Supplementary Fig. 1)[60]. While these contacts are observed in all SENP/ULP family members and are essential for the SUMO specificity over other UbLs, they do not alone determine SENP5's SUMO2 preference[25,28–30,52,53].

Among all SENP5$_{CD}$ interface contacts with SUMO1 and SUMO2, Asn607 and Arg624 stand out as potential determinants of SENP5's SUMO2 preference. Asn607 forms a hydrogen bond with the carbonyl oxygen of Gly64 (SUMO2) or Gly68 (SUMO1), and in SUMO2 also with the guanidinium group of Arg61 (Figs. 3c and 4a). In SENP2 and SENP7, Asn607 is replaced by serine, preventing its involvement in the interface (PDB IDs 7R2E and 2IO0, respectively)[29,52] (Fig. 2e).

Arg624, located within the α-helix α4, forms electrostatic interactions with Asp63 and Asp82 of SUMO2 in the SENP5$_{CD}$-SUMO2 complex (bond distances: 2.8 Å and 3.2 Å, respectively) (Figs. 3, 4a and Supplementary Fig. 5). These interactions are absent in the SENP5$_{CD}$-SUMO1 complex (Figs. 3, 4a and Supplementary Fig. 5). Arg624 is conserved in SENP1 and SENP2 but replaced by threonine in SENP6 and SENP7 (Fig. 2e and Supplementary Fig. 1). Interestingly, the presence of glutamic acid in SUMO1 (Glu67) or aspartic acid in SUMO2 (Asp63) at the same interface position may influence Arg624's orientation, facilitating the electrostatic interaction in SUMO2. This difference could contribute significantly to SENP5's preference for SUMO2.

Major role of Arg624 in the SENP5$_{CD}$ selectivity for SUMO2 substrates

In vitro activity assays using SENP5$_{CD}$ N607A, R624A, and K627A point mutants with both fluorogenic substrates (SUMO1-AMC and SUMO2-AMC) and model conjugated substrates (RanGAP1-SUMO1 and RanGAP1-SUMO2) revealed distinct effects on isopeptidase activity (Fig. 4b, c). While the N607A and K627A mutants impair activity for both SUMO1 and SUMO2 substrates, the R624A mutation only decreases the deconjugation activity for SUMO2 substrates. SENP5$_{CD}$ R624A exhibits a significant decrease in activity with all tested SUMO2 substrates but maintains comparable activity toward SUMO1 substrates compared to wild-type SENP5$_{CD}$.

To further investigate SENP5's deconjugation activity in a cellular context, we analyzed SUMO1 and SUMO2 deconjugation assays in HEK293F and COS-7 cells (Fig. 4d and Supplementary Fig. 6). HEK293F suspension cells were co-transfected with full-length SENP5 wild-type, C713A active site mutant, R624A single and R624A/K627A double point mutant, together with the Fl-PML substrate (Fig. 4d) and endogenous SUMO isoform conjugates were checked with either SUMO1 and SUMO2 antibodies. Western blot analysis of cellular extracts 4 days after transfection display a significant decrease of endogenous SUMO2 conjugates in SENP5 WT compared to SENP5 C713A, R624A, and R624A/K627A point mutants, supporting the role of Arg624 in the deconjugation activity. On the other hand, immunoblot analysis of similar extracts with SUMO1 antibody does not show significant differences between WT and the point mutants, probably indicating a poor activity of SENP5 for SUMO1-conjugates in HEK293F cells. Analogous results are observed in COS-7 cells co-transfected with HA-SUMO1 or HA-SUMO2, but in this instance we could only compared the different levels of unbound HA-SUMO2 (Supplementary Fig. 6).

All these activities suggest that the electrostatic interactions mediated by Arg624, particularly with Asp63 of SUMO2, plays a crucial role in enhancing SENP5's preference for SUMO2 over SUMO1 conjugates.

Swapping the SUMO isoforms activities in SENP5$_{CD}$

To further investigate the role of electrostatic interactions in SUMO isoform preference, we generated point mutations (SUMO1 E67D and SUMO2 D63E) that swapped the countercharge partner for Arg624 in

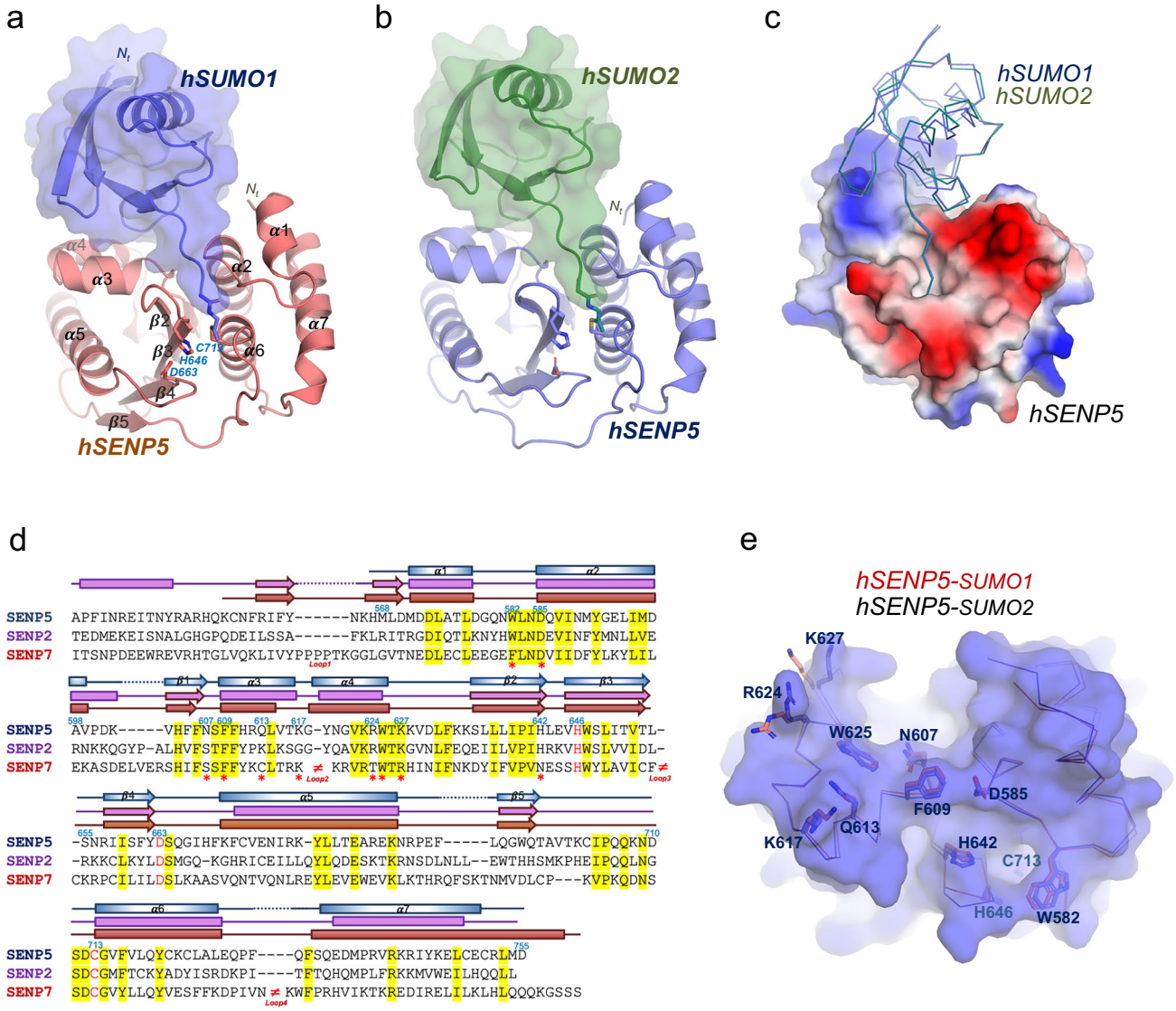

Fig. 2 | Crystal structure of the complex of human SENP5$_{CD}$ with SUMO1 and SUMO2. a Cartoon representations of the SENP5$_{CD}$-SUMO1 complex structure. SENP5 catalytic domain and SUMO1 are shown in orange and blue, respectively. The catalytic residues are labelled and depicted in stick representation. Secondary structure elements are labelled. N-terminal and C-terminal are marked. **b** Cartoon representations of the SENP5$_{CD}$-SUMO2 complex structure. SENP5 catalytic domain and SUMO1 are shown in blue and green, respectively. The catalytic residues are labelled and depicted in stick representation. Secondary structure elements are labelled. N-terminal and C-terminal are marked. **c** Structural superimposition between SENP5$_{CD}$-SUMO1 (blue) and SENP5$_{CD}$-SUMO2 (green) complexes. SENP5$_{CD}$ is depicted as an electrostatic surface representation. **d** Structural alignment of sequences corresponding to the catalytic domains for human SENP2, SENP5 and SENP7. Red asterisks indicate interface residues with SUMO2. Catalytic triad residues are shown in red. Secondary structure cartoon is depicted above for SENP5 (green), SENP2 (violet) and SENP7 (brown). **e** Superposition of the SENP5$_{CD}$ structures (blue surface) in complex with SUMO1 (red) or SUMO2 (blue). Side chain interface residues are depicted in a stick representation.

SUMO1 and SUMO2 (Fig. 5). These mutations introduce a key chemical difference: the presence of an additional methylene group in the glutamate side chain compared to aspartate. We hypothesized that this alteration might contribute to the lower deconjugation activity observed with all tested SUMO1 substrates.

Strikingly, the SUMO1 E67D mutation enhances its deconjugation activity toward RanGAP1 conjugates compared to wild-type SUMO1, which is nearly inactive. Conversely, the SUMO2 D63E mutation significantly reduces RanGAP1 deconjugation activity (Fig. 5a). Fluorogenic SUMO-Rhodamine confirmed these results, displaying similar activities for SUMO2-Rho D63E and SUMO1-Rho E67D, with a notable gain of activity for SUMO1 mutant compared to the loss for SUMO2 mutant (Fig. 5b).

Following our initial competitive kinetics assay (Fig. 1c), we investigated the impact of these swapping mutations using a similar approach. We measured the decrease in SUMO2-Rho activity upon competition with RanGAP1 conjugated to either SUMO1 E67D or SUMO2 D63E (Fig. 5c). The IC_{50} for RG-SUMO2 D63E significantly increased from 3.7 μM to 56.4 μM compared to wild-type SUMO2, indicating a roughly 15-fold decrease in its inhibitory activity. Conversely, the IC_{50} for RG-SUMO1 E67D, which was undetectable for wild-type SUMO1, became measurable at around 87.2 μM, quite similar to RG-SUMO2 D63E.

Human SENP3, the closest homolog of SENP5, has been suggested to share functional overlap[50,59]. Consistent with SENP5 results, full length SENP3 preferentially binds SUMO2-derived activity-based probe (ABP) (Fig. 5d). While SENP3 showed a slight binding increase against SUMO1 E67D, it exhibited decreased binding against SUMO2 D63E compared to their wild-type counterparts. These findings reinforce the importance of Arg624 in mediating SUMO2/3 selectivity for both SENP3 and SENP5, thus broadening the significance of our results.

https://doi.org/10.1038/s41467-025-60029-4

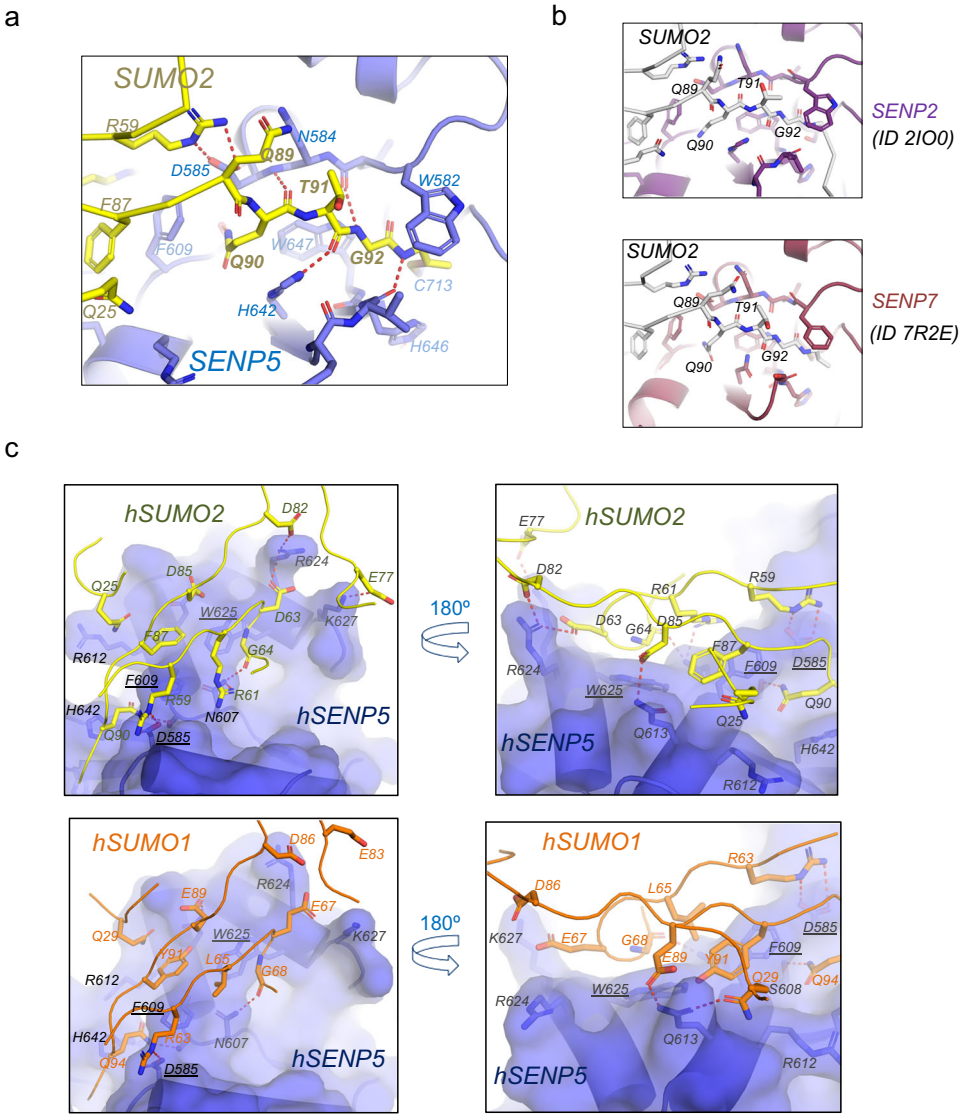

Fig. 3 | Structural details of the SENP5$_{CD}$ complex with SUMO1 and SUMO2. **a** Close-up view of the C-terminal tail of human SUMO2 (yellow) in complex with SENP5$_{CD}$ (blue). Binding side-chain residues in the contact area of substrate and enzyme are shown in stick representation and labelled. Hydrogen bonds are represented by dashed red lines. **b** Similar close-up views of the C-terminal of SUMO2 (gray) in complex with SENP2 (upper) and SENP7 (below). **c** (Upper) Close-up view of the ribbon representation of SENP5$_{CD}$-SUMO2 interface in two orthogonal views. Binding side-chain residues in the contact area are labelled and shown in stick representation. Hydrogen bonds and charged interactions are represented by dashed red lines. (Below) Similar close-up view of the ribbon representation of SENP5$_{CD}$-SUMO1 interface in two orthogonal views.

The crystal structure of SUMO1E67D resembles the SUMO2 interface to SENP5$_{CD}$

Moreover, to further investigate the molecular mechanism behind the SUMO1 E67D enhancement, we successfully crystallized and solved the structure of SENP5$_{CD}$ in complex with the SUMO1 E67D mutant at 1.73 Å resolution (Table 1) (Fig. 5e, f). Electron density maps of the complex interface validated our hypothesis regarding the role of Arg624, revealing the presence of electrostatic contacts between Arg624 and Lys627 with Asp67 in the SUMO1 mutant, resembling those observed in the SENP5$_{CD}$-SUMO2 complex (Suppementary Figs. 5 and 7). However, these interactions were absent in wild-type SUMO1, where Glu67 is present. Furthermore, the overall structural alignment of wild-type and E67D SUMO1 revealed a significant backbone shift, positioning the mutant closer to the SUMO2 interface (Fig. 5g).

Our findings suggest that the electrostatic interaction between Arg624 in SENP5$_{CD}$ and Asp63 in SUMO2 contributes to SENP5's higher proteolytic activity toward SUMO2 conjugates. The shorter side chain of aspartate compared to glutamate in SUMO1, may allow for the optimal positioning and distance required for a stronger electrostatic interaction with arginine, potentially enhancing SUMO2 binding and subsequent proteolytic processing by SENP5$_{CD}$.

Discussion

The human SENP/ULP family of SUMO isopeptidases can be classified into three subgroups based on structural and sequence analysis: SENP1-2, SENP3-5, and SENP6-7. Excluding the divergent SENP8/NEDP1, which is specific for Nedd8[61], all other SENP members exhibit SUMO isopeptidase activity[29,30,52,54]. While SENP1 and SENP2 exhibit activity toward both SUMO isoforms, the remaining subgroups, SENP3-5 and SENP6-7, demonstrate a strong preference for the SUMO2 isoform as determined by in vitro deconjugation assays. Within the SENP6-7 subgroup, long insertions are present in the middle of the catalytic domain, including the "Loop1" insertion, which we identified as a key determinant of SUMO2/3 substrate specificity[25,52–54]. In contrast, the specificity of SENP3 and SENP5 for SUMO2/3 isoforms likely arises

https://doi.org/10.1038/s41467-025-60029-4

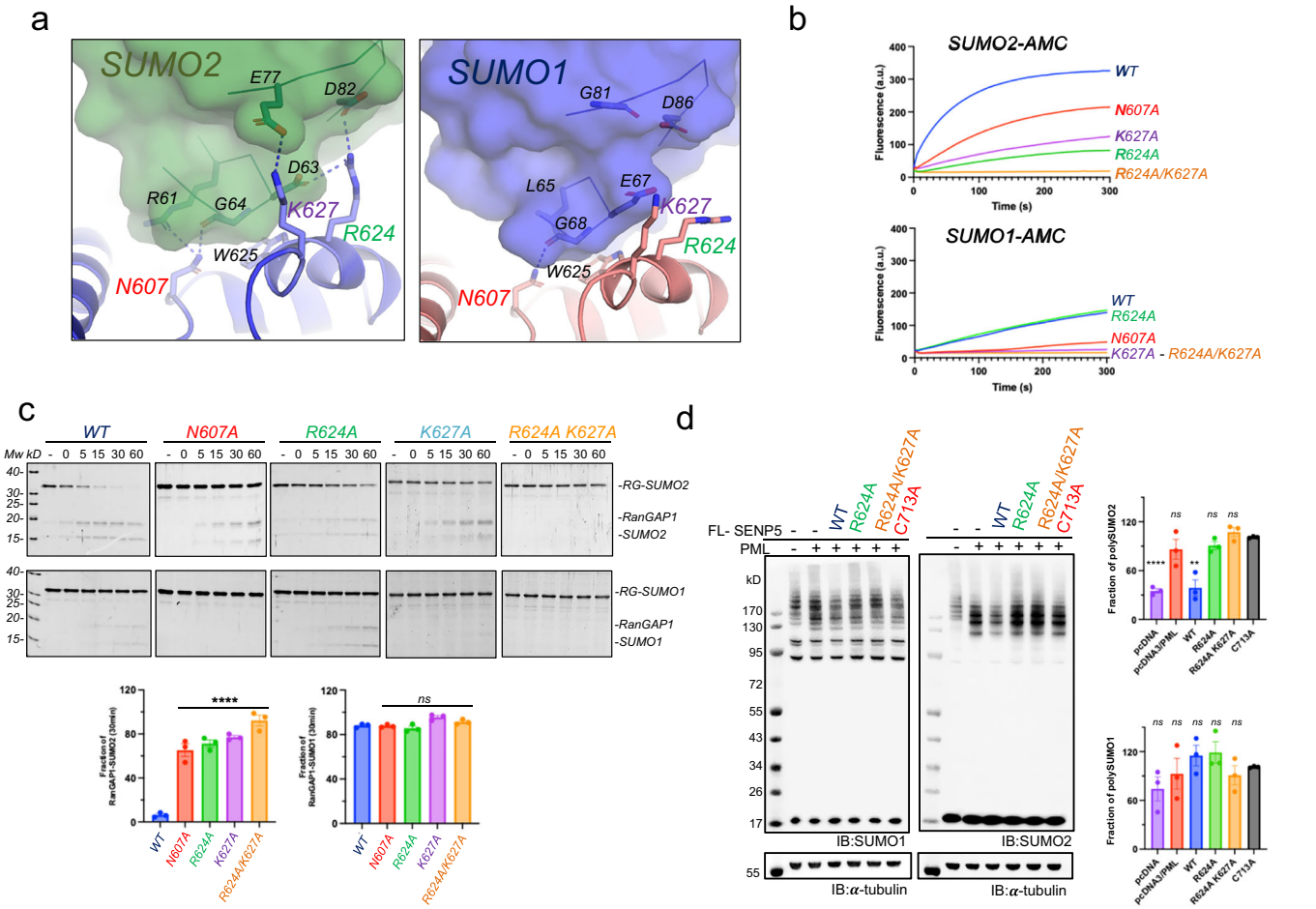

Fig. 4 | Analysis of the SENP5 point mutants. a Close-up view of the ribbon representation of interfaces of $SENP5_{CD}$-SUMO2 (green) and $SENP5_{CD}$-SUMO1 (blue) around Asn607 and Arg624. Interface residues are labelled and shown in stick representation. **b** Plot of the proteolytic cleavage of SUMO1-AMC and SUMO2-AMC to test the activity of $SENP5_{CD}$ wild type and $SENP5_{CD}$ N607A, R624A, K627A, and R624/K627A mutants. SUMO2-AMC was incubated with $SENP5_{CD}$, and released AMC was identified by fluorescence. The plot is an average of a triplicate experiment. **c** SDS-PAGE of the endpoint assays of $SENP5_{CD}$ wild type and $SENP5_{CD}$ N607A, R624A K627A, and R624/K627A mutants using RanGAP1-SUMO1 and RanGAP1-SUMO2 substrates. (*Below*) Plot of the fraction of the RanGAP1-SUMO2 and RanGAP1-SUMO1 substrate after 30 min reaction. Data values represent the mean ± SEM, $n = 3$ technical replicates. Significance was measured by a two-tailed unpaired *t* test relative to wild-type. All data were analyzed with a 95% confidence interval. $^{*}P \le 0.05$, $^{**}P \le 0.01$, $^{***}P \le 0.001$, $^{****}P \le 0.0001$. Exact *P* values from left to right: 0.0005, <0.0001, <0.0001, and <0.0001. **d** Western Blot analysis of HEK293F cells co-transfected with Flag-PML and either the empty pcDNA3 (−) or the plasmids expressing full-length SENP5, SENP5-R624A, SENP5-C713A or SENP5-R624A/K627A. (*left*) Immunoblot showing the levels of endogenous SUMO1 and SUMO2 in HEK293F cells. Anti-SUMO1 and antiSUMO2 antibodies were used to detect both endogenous SUMO isoforms. Anti-tubulin antibody was used as a loading control. (*right*) Plot of the Western Blot triplicate showing the fraction of polySUMO conjugates for each experiment regarding to SENP5 active site mutant (C713A). Data values represent the mean ± SEM, $n = 3$ technical replicates. Significance was measured by a two-tailed unpaired *t* test relative to C713A mutant. All data were analyzed with a 95% confidence interval. $^{*}P \le 0.05$, $^{**}P \le 0.01$, $^{***}P \le 0.001$, $^{****}P \le 0.0001$. Exact *P* values from left to right: <0.0001 and 0.0032. Source data are provided as a Source Data file.

from interactions other than "Loop1", which they lack. To elucidate the structural basis for SUMO2 isoform preference in SENP5, we have compared the crystal structures of $SENP5_{CD}$ in complex with either SUMO1 or SUMO2.

Full-length SENP/ULP family members consist of a long, structurally disordered N-terminal extension followed by a conserved catalytic domain. The catalytic domain adopts a characteristic CE-clan cysteine protease fold[18]. While the precise function of the disordered N-terminal extensions remains to be fully elucidated, available evidence suggests that they may play roles in several aspects of SENP/ULP biology[24,31–34]. These extensions could potentially contribute to the subcellular localization of SENP/ULP members or facilitate the binding of specific protein targets within the cell.

Cellular functions attributed to the non-catalytic disordered regions in substrate recruitment have been reported for SENP6 and SENP7. For instance, the presence of seven SIM (SUMO-Interacting motif) domains within the disordered region of SENP7 has been shown to play a crucial role in the recruitment of polySUMOylated KAP1 (Karyopherin 1) during homologous recombination[62]. The disordered region of SENP6 also contains multiple SIM motifs, enabling it to recruit polySUMOylated targets for deconjugation[24,63,64]. Additionally, the yeast ULP2, a SENP6 homolog, possesses multiple SIM motifs in its N-terminal disordered region[24]. This suggests a conserved role for SIM motifs in the recruitment of polySUMOylated substrates by SENP/ULP family members[65]. In the SENP3 and SENP5 subfamily, the non-structured N-terminal region has primarily been implicated in subcellular localization[40,46,51,55]. Despite their length and structural disorder, the N-terminal extensions of all SENP/ULP family members appear to be dispensable for catalytic activity, including the ability to dismantle polySUMO2 chains. The catalytic activity of these enzymes is solely confined to their conserved CE-clan catalytic domains.

Structural analysis of $SENP5_{CD}$ complexes with SUMO1 and SUMO2 reveals a smaller interface with SUMO compared to $SENP1_{CD}$, $SENP2_{CD}$, and $SENP7_{CD}$ (Supplementary Fig. 4). Despite its reduced

https://doi.org/10.1038/s41467-025-60029-4

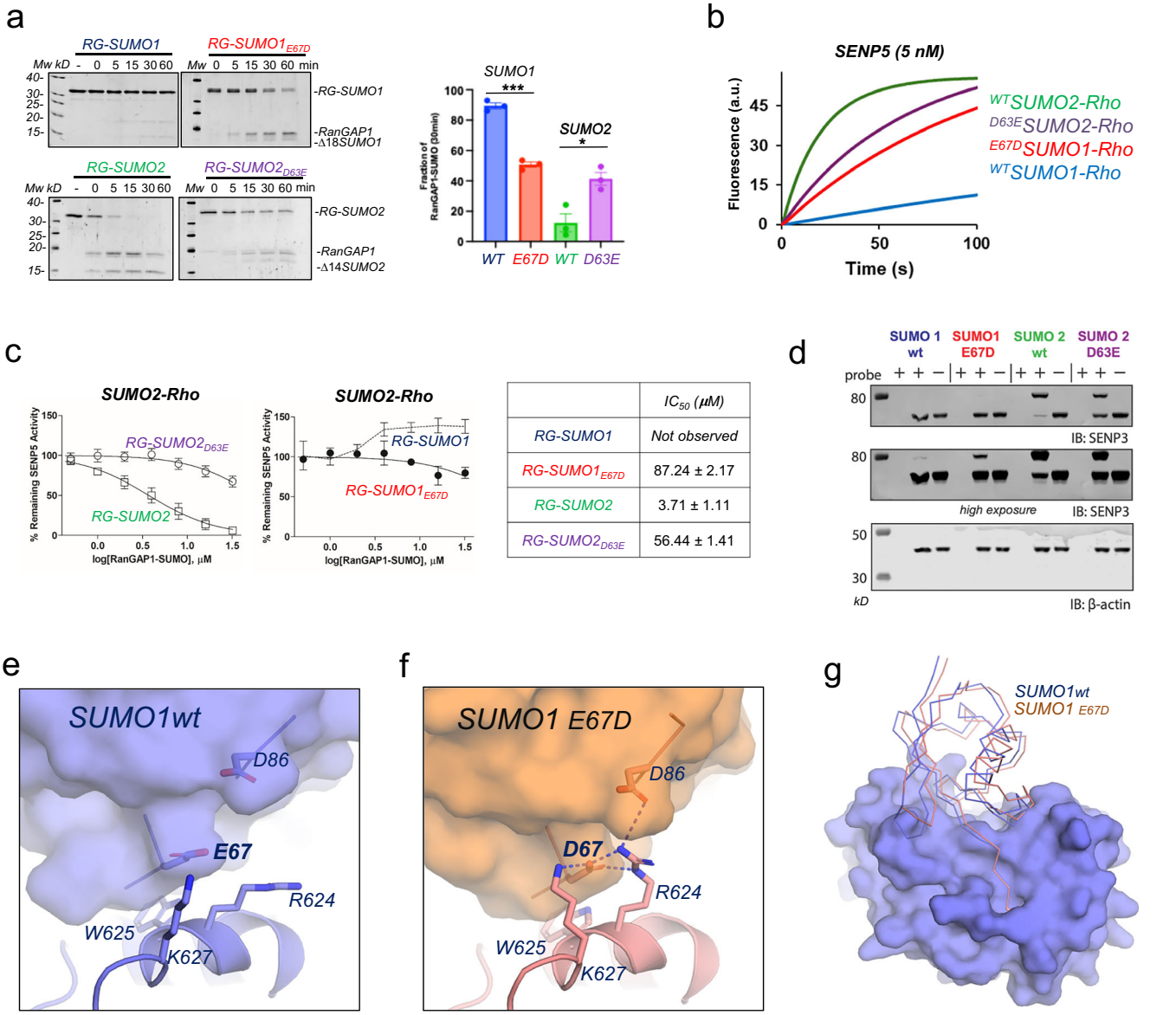

Fig. 5 | Analysis of the swapping activities of SENP5 for SUMO1 and SUMO2 substrates. a SDS-PAGE of the endpoint assays of $SENP5_{CD}$ using the RanGAP1-SUMO1 and RanGAP1-SUMO2 wild types, and RanGAP1-SUMO1 E67D and RanGAP1-SUMO2 D63E point mutants as substrates. (*Right)* Plot of the fraction of the RanGAP1-SUMO1 wild type and point mutants after 30 min reaction. Data values represent the mean ± SEM, $n = 3$ technical replicates. Significance was measured by a two-tailed unpaired t test relative to wild-type. All data were analyzed with a 95% confidence interval. $^{*}P \le 0.05$, $^{**}P \le 0.01$, $^{***}P \le 0.001$, $^{****}P \le 0.0001$. Exact P values from left to right: 0.0001 and 0.0173. **b** Plot of the proteolytic cleavage of SUMO1-Rho, SUMO2-Rho wild types and SUMO1-Rho E67D and SUMO2-Rho D63E point mutants to test the activity of $SENP5_{CD}$. The plot is an average of a triplicate experiment. **c** Plot of a competition assay by measuring the interference of the $SENP5_{CD}$ activity for SUMO2-Rhodamine substrate by competition with RanGAP1-SUMO1 and RanGAP1-SUMO2 wild types, and RanGAP1-SUMO1 E67D and RanGAP1-SUMO2 D63E point mutants at different concentrations. (*Right*) Inhibitory constant values (IC_{50}) for RanGAP1-SUMO1 and RanGAP1-SUMO2 wild types, and RanGAP1-SUMO1 E67D and RanGAP1-SUMO2 D63E point mutants substrates on the $SENP5_{CD}$ wild type activity on SUMO2-Rhodamine fluorogenic substrate. Data values represent the mean ± SEM, $n = 3$ technical replicates. **d** Immunoblot analysis of the labeling of endogenous full length human SENP3 in HEK293T lysates with activity-based probes of either SUMO1 or SUMO2 wild type and point mutants. Anti-actin antibody was used as a loading control. $n = 3$ technical replicates. **e** Close-up view of the ribbon representation of interfaces of $SENP5_{CD}$-SUMO1 wild type depicting the basic patch region around Arg624. Interface residues are labelled and shown in stick representation. **f** Close-up view of the ribbon representation of interfaces of $SENP5_{CD}$-SUMO1 E67D point mutant depicting the basic patch region around Arg624. **g** Superposition of the SENP5 structures (blue surface) in complex with SUMO1 wild type (blue ribbon) or SUMO1 E67D (orange ribbon). Source data are provided as a Source Data file.

size, this interface is sufficient to confer SUMO2/3 specificity over SUMO1. In addition to the common SUMO contacts observed in all members of the SENP/ULP family, such as the conserved C-terminal tail and essential residues in the globular domain (Asp585, Phe609, and Trp625), the $SENP5_{CD}$ interface features unique contacts that may contribute to its preference SUMO2/3. One such feature is a basic patch centered around Arg624.

The relatively smaller interface between $SENP5_{CD}$ and SUMO2 compared to $SENP1_{CD}$, $SENP2_{CD}$, or $SENP7_{CD}$ may amplify the effects of single point mutations on deconjugation activity, as observed in our analysis of the $SENP5_{CD}$ N607A, K627A, and R624A point mutants. These positions were chosen, particularly N607A and R624A, because they engage in unique interactions with SUMO2, compared to SUMO1. Surprisingly, whereas disruption of Asn607 decreases the $SENP5_{CD}$

activity for both SUMO isoforms, Arg624 has a strong decrease of deconjugating activity only for SUMO2 substrates. Arg624 in $SENP5_{CD}$ forms a well-oriented salt bridge interaction with Asp63 and Glu77 in SUMO2. However, in SUMO1, the equivalent Asp63 position is replaced by a glutamate residue. Due to its longer side chain, glutamate is unable to properly accommodate Arg624, preventing the formation of the electrostatic interaction observed in complex with SUMO2, but absent in the SUMO1 complex.

Interestingly, a similar electrostatic interaction between Arg624 and SUMO2 residues can be observed in the $SENP2_{CD}$-SUMO2 complex structure (PDB code 2IO0)[29]. However, this interaction is absent in the $SENP2_{CD}$-SUMO1 complex (PDB code 1TGZ)[28], where the arginine side chain is oriented outwards, resembling the conformation seen in our $SENP5_{CD}$-SUMO1 complex. Despite the presence of this electrostatic interaction in $SENP2_{CD}$-SUMO2, SENP2 does not exhibit a strong preference for either SUMO1 or SUMO2. This suggests that the larger number of interface contacts in $SENP2_{CD}$-SUMO complexes may compensate for the absence of the arginine-SUMO1 interaction, mitigating its effect on isoform specificity.

In addition to their well-known roles in eukaryotic systems, CE-clan proteases, such as SENP5, have been identified in infectious bacteria and viruses, raising intriguing questions about their evolution and function. Given that most prokaryotes lack conventional ubiquitin or UBLs, the presence of bacterial CE-clan proteases targeting ubiquitin conjugates is particularly notable[66–68]. This adaptation expands the substrate specificity of the canonical catalytic domain, enabling bacteria to manipulate the host's ubiquitin and UBL signaling pathways. Such modifications likely enhance bacterial survival and persistence within the host. In bacterial CE-clan proteases, specificity for ubiquitin and UBLs is mainly regulated by changes in three connecting loops (VR1-3) at the interface with the ubiquitin or UBL moiety[67]. In contrast, SENP5's specificity for SUMO2 is primarily determined by a basic patch surrounding Arg624, located in the VR-2 loop, while SENP7 recognizes SUMO2 through the Loop1 insertion in the VR-1 loop. These differences illustrate the remarkable adaptability of CE-clan proteases and their diverse strategies for achieving substrate specificity.

The human SENP family plays a pivotal role in regulating a variety of cellular processes, and their dysregulation is implicated in numerous diseases, including cancer, neurodegenerative disorders, and cardiovascular diseases. Recent reviews have emphasized the critical involvement of SENP proteases in tumorigenesis, highlighting their role in the disruption of cellular signaling pathways[8,69]. Given the importance of SENPs in cellular regulation, understanding the molecular mechanisms behind their substrate specificity, particularly the preference for SUMO isoforms, is essential. This insight could facilitate the development of highly specific inhibitors and probes targeting individual SENP family members, offering new therapeutic opportunities with minimal off-target effects.

Methods

Plasmids, cloning and point mutation

$SENP5_{CD}$ catalytic domain (aa 568–755) was amplified from human cDNA library and cloned into a pET28a vector. Restriction Enzyme Free PCR was used to clone the PTXB1-Δ14-humanSUMO2-intein-chitin-binding domain (CBD) (14 residues N-terminal deletion)[70]. Point mutants of SENP5, SUMO1, and SUMO2 were performed by site-directed mutagenesis[71]. Full-length RGS-SENP5 was a gift from Edward Yeh (Addgene plasmid #18053; http://n2t.net/addgene:18053; RRID:Addgene_18053), pLPC-Flag-PML-IV was a gift from Gerardo Ferbeyre (Addgene plasmid #62804; http://n2t.net/addgene:62804; RRID:Addgene_62804), pcDNA3-HA-SUMO1 was a gift from Junying Yuan (Addgene plasmid #21154; http://n2t.net/addgene:21154; RRID:Addgene_21154) and pcDNA3 HA-SUMO2 WT was a gift from Guy Salvesen (Addgene plasmid #48967; http://n2t.net/addgene:48967; RRID:Addgene_48967)[38,72–74]. The primers used for these experiments are shown in Supplementary Table 1. Final constructs were verified by DNA sequencing.

Protein expression and purification

$SENP5_{CD}$ (aa 568 to 755) and Δ14SUMO2 expression constructs were expressed in *E. coli* Rosetta (DE3) cells (Novagen) for 5 h at 30 °C after induction with 0.5 mM IPTG. $SENP5_{CD}$ suspension was equilibrated in 350 mM NaCl, 20 mM Tris-HCl (pH 8.0), 10 mM imidazole, 20% sucrose, 1 mM BME (*β-mercaptoethanol*), and 0.1% IGEPAL CA-630, and cells were sonicated to break. Nickel affinity chromatography was used to purify $SENP5_{CD}$ via the N-terminal HIS-tag from the pET28 vector. Proteins were further separated by gel filtration chromatography (Superdex 75 26/60; Cytiva) with buffer 250 mM NaCl, 20 mM Tris 8.0, 1 mM BME.

For Δ14-SUMO2 PA protein purification, 60 mL chitin beads were prepared (New England Biolabs, UK), previously washed with 5CV (column volume) (1CV = 200 mL) cold lysis buffer (50 mM HEPES 8.0, 50 mM NaCl) in 4 degrees. Four liters of Δ14SUMO2-intein-CBD pellet are resuspended in 200 mL lysis buffer. After being sonicated, the 200 mL supernatant is filtered through a 0.45 µm nylon membrane filter, placed into the chitin column and gently shaken overnight at 4 °C. To remove unbound proteins, the column was washed at 4 °C with 5CV lysis buffer. Then 200 mL of lysis buffer containing 150 mM MesNa was added and gently shaken for 48 h at room temperature. The remaining product was collected by adding 15 mL lysis buffer to the 200 mL flow-through. Eluted sample was concentrated to 30 mL with a 3 kDa filter and dialyzed overnight at 4 °C. After dialysis, 150 mM Propargylamine was added to the 30 mL product for 4 and 5 h at room temperature. The product was dialyzed overnight at 4 °C, concentrated to remove precipitate and applied to an anion exchange resin (Resource Q 6 mL; GE Healthcare). Elution was performed with a 0–1 M NaCl gradient from 0 to 50% in 20 mM Tris-HCl (pH 8.0) and 1 mM BME.

Synthesis of Δ18 N SUMO1 wild-type and E67D PA

SUMO1 E67D (ΔN; 18 to C-term) was obtained by standard 9-fluorenylmethoxycarbonyl (Fmoc) based solid phase peptide chemistry on trityl-resin as described in literature on a 20 mmol scale[56]. The N-terminus was protected by treating the resin with Di-tert-butyl dicarbonate (21.8 mg, 100 µmol, 5.0 eq.) and DIPEA (34.84 µl, 200 µmol, 10.0 eq.) in DMF (2 ml) for 3 h. Sidechain protected SUMO was released from the resin by treatment with 1,1,1,3,3,3-hexafluoropropan-2-ol (HFIP)/DCM (2.5 ml, 1/4, v/v) for 3 × 20 min, after which it was filtered and the solvent was removed by rotary evaporation. Residual HFIP was removed by co-evaporation 2–3 times with DCE (to prevent formation of HFIP ester in next steps) and dried to use in the next step. The SUMO protein was dissolved in DCM (5 mL) and to this were added propargyl amine (13 µL, 200 µmol, 10 eq), PyBOP (52 mg, 100 µmol, 5.0 eq) and TEA (14 µL, 100 µmol, 5.0 eq), upon which the mixture was stirred at rt for 16 h. The mixture was concentrated under reduced pressure and the SUMO polypeptide sequence was dissolved in a mixture of TFA/H_2O/TIPS/phenol (90.5/5/2/2.5 v/v/v/v; 5 mL) and stirred for 4 h at rt towards global deprotection. The protein was precipitated with ice-cold Et_2O/*n*-pentane (3/1; v/v; 40 mL). The precipitated protein was isolated by centrifugation and washed by three cycles of resuspension in ice-cold diethyl ether and centrifugation. The pellet was dissolved in H_2O/MeCN/FA (75/24/1; v/v/v; 20 mL) and lyophilized. The crude product was purified using RP-HPLC and relevant fractions were pooled and lyophilized to afford ΔN SUMO1 E67D PA as a white solid (Supplementary Fig. 8).

Synthesis of SUMO-Rhodamine-Morpholine (RM) reagents

SUMO1/2 wild-type or mutant (SUMO1 E67D and SUMO2 D63E) were obtained by standard 9-fluorenylmethoxycarbonyl (Fmoc) based solid phase peptide chemistry on trityl-resin as described

in literature on a 20 mmol scale[56]. The N-terminus was protected by treating the resin with Di-tert-butyl dicarbonate (21.8 mg, 100 μmol, 5.0 eq.) and DIPEA (34.84 μl, 200 μmol, 10.0 eq.) in DMF (2 ml) for 3 h. Sidechain protected SUMO was released from the resin by treatment with 1,1,1,3,3,3-hexafluoropropan-2-ol (HFIP)/DCM (2.5 ml, 1/4, v/v) for 3 × 20 min, after which it was filtered and the solvent removed by rotary evaporation. Residual HFIP was removed by co-evaporation 2–3 times with DCE (to prevent formation of HFIP ester in next steps) and dried to use in the next step. The SUMO protein was dissolved in DMF (5 mL) and to this were added EDC HCl (18 mg, 10 μmol, 5.0 eq), HOBt monohydrate (15 mg, 100 μmol, 5.0 eq) and GlyRM[75] (20 mg, 40 μmol, 2.0 eq), upon which the mixture was stirred at rt for 16 h. The mixture was concentrated under reduced pressure and the SUMO polypeptide sequence was dissolved in a mixture of TFA/H_2O/TIPS/phenol (90.5/5/2/2.5 v/v/v/v; 5 mL) and stirred for 4 h at rt towards global deprotection. The protein was precipitated with ice-cold Et_2O/*n*-pentane (3/1; v/v; 40 mL). The precipitated protein was isolated by centrifugation and washed by three cycles of resuspension in ice-cold diethyl ether and centrifugation. The pellet was dissolved in H_2O/MeCN/FA (75/24/1; v/v/v; 20 mL) and lyophilized. The purity of the peptides was determined by LC-MS analysis. The crude product was purified using RP-HPLC and relevant fractions were pooled and lyophilized to afford the SUMO peptides as white solids (Supplementary Figs. 9 and 10).

Synthesis of SUMO propargylamide activity-based probes

SUMO1/2 wild type or mutant (S1 E67D, S2 D63E) were obtained by standard 9-fluorenylmethoxycarbonyl (Fmoc) based solid phase peptide chemistry on trityl-resin as described in literature on a 20 mmol scale. A solution of Fmoc-PEG2-COOH (39 mg, 100 μmol, 5.0 eq), PyBOP (52 mg, 100 μmol, 5.0 eq), and DIPEA (36 μL, 200 μmol, 10 eq) in NMP was shaken for 10 min and added to the SUMO on resin for 3 h at room temperature. After completion, the resin was washed alternately with NMP (3 × 5 mL) and DCM (3 × 5 mL). The resin was treated with piperidine/NMP (4 mL, 1/4, v/v) for 2 × 20 min. A solution of Fmoc-Lys(biotinyl)-OH (59 mg, 100 μmol, 5.0 eq), PyBOP (52 mg, 100 μmol, 5.0 eq) and DIPEA (36 μL, 200 μmol, 10 eq) in NMP was shaken for 10 min and added to the SUMO on resin for 3 h at room temperature. After completion, the resin was washed alternately with NMP (3 × 5 mL) and DCM (3 × 5 mL). The resin was treated with piperidine/NMP (4 mL, 1/4, v/v) for 2 × 20 min. A solution of Boc_2Rho (34 mg, 60 μmol, 3.0 eq), PyBOP (52 mg, 100 μmol, 5.0 eq), and DIPEA (36 μL, 200 μmol, 10 eq) in NMP was shaken for 10 min and added to the SUMO on resin for 3 h at room temperature. After completion, sidechain protected Rho/Bio-SUMO dG was released from the resin by treatment with 1,1,1,3,3,3-hexafluoropropan-2-ol (HFIP)/DCM (2.5 ml, 1/4, v/v) for 3 × 20 min, after which it was filtered and the solvent was removed by rotary evaporation. Residual HFIP was removed by co-evaporation 2–3 times with DCE (to prevent formation of HFIP ester in next steps) and dried to use in the next step. The SUMO protein was dissolved in DMF (5 mL) and to this were added propargyl amine (6.4 μL, 100 μmol, 5.0 eq), EDC HCl (19.2 mg, 100 μmol, 5.0 eq) and HOBt (15.2 mg, 100 μmol, 5.0 eq), upon which the mixture was stirred at rt for 16 h. The mixture was concentrated under reduced pressure and the SUMO polypeptide sequence was dissolved in a mixture of TFA/H_2O/TIPS/phenol (90.5/5/2/2.5 v/v/v/v; 5 mL) and stirred for 4 h at rt towards global deprotection. The protein was precipitated with ice-cold Et_2O/*n*-pentane (3/1; v/v; 40 mL The precipitated protein was isolated by centrifugation and washed by three cycles of resuspension in ice-cold diethyl ether and centrifugation. The pellet was dissolved in H_2O/MeCN/FA (75/24/1; v/v/v; 20 mL) and lyophilized. The protein was purified using RP-HPLC to afford the Rho/Bio-SUMO PA probes as pink solids (Supplementary Figs. 11 and 12).

Generation of SENP5-SUMO complexes

SENP5 Δ568 protein was incubated with Δ14SUMO2-PA, Δ18SUMO1-PA or Δ18SUMO1E67D-PA (1:3 ratio) in a buffer containing 250 mM NaCl, 20 mM Tris 8.0, 3 mM DTT for 2 h at 37 °C. The protein buffer was exchanged to 50 mM NaCl, 20 mM Tris 8.0, 1 mM DTT and applied to an cation exchange resin (Resource S 6 mL; GE Healthcare).

Crystallization, data collection and refinement

The complexes of $SENP5_{CD}$ with Δ14SUMO2 PA, Δ18SUMO1 PA or Δ18SUMO1E67D PA were finally concentrated to 9.5 mg/mL, 3.5 mg/mL and 6.6 mg/mL, respectively for crystallization in a buffer composed by 60 mM NaCl, 8 mM Tris 8.0, 1 mM BME. Crystallization was performed at 18 °C by sitting drop vapor diffusion method by mixing protein with an equal volume of a screen condition solution containing 0.1 M Sodium HEPES 7.0, 15 % w/v PEG 20,000 for SUMO2, 2.1 M DL-Malic acid pH 7.0 for SUMO1 or 0.2 M Lithium sulfate, 0.1 M Sodium acetate 5.5, 8 % w/v PEG 20,000 and 8 % v/v PEG 500 MME for SUMO1E67D. After 1 week, the crystals were harvested and soaked for 10 s in 15% ethylene glycol before flash freezing in liquid nitrogen.

Diffraction data were collected to 2.36 Å, 1.73 Å, and 2.18 Å resolution for SUMO1, SUMO1E67D, and SUMO2 complexes, respectively, at the ALBA synchrotron beamline BL13-XALOC (Barcelona, Spain)[76] (Table 1). Data was processed, scaled, reduced, and further analyzed with the automatic autoPROC software package[77] including XDS, POINTLESS, AIMLESS, CCP4, and STARANISO. Crystallographic details are summarized in Table 1.

The structure of $SENP5_{CD}$-Δ14SUMO2, $SENP5_{CD}$-Δ18SUMO1, and $SENP5_{CD}$-Δ18SUMO1E67D was solved by molecular replacement using SENP5 AlphaFold-2 model and SUMO2 (1WM3) or SUMO1 (1TGZ) as search models with Phaser. Following rounds of model building and refinement were carried out with Coot and Phenix[78,79] (Table 1).

Transient cell transfection

HEK293F cells were maintained at 37 °C in FreeStyle™ 293 Expression Medium (Gibco, Life Technologies). Cells were seeded at a density of 0.5×10^6 cells/mL in a final volume of 2 mL per well in a 6-well plate. The cells were incubated for 24 h in an orbital shaker incubator at 37 °C, and a humidified atmosphere with 8% CO_2 until they reached a density of 1.0×10^6 cells/mL. Subsequently, the cells were co-transfected with 1 μg of DNA per 1 mL of final cell culture using a 1:3 (w/w) ratio of DNA to polyethylenimine (PEI linear, 25,000 Da, Polysciences, Warrington, PA, USA). The cells were then incubated in an orbital shaker for 96 h at 37 °C, 120 rpm, and 8% CO_2. After 96 h, the cells were harvested by centrifugation at 3000 × *g* for 5 min. Lysis was performed using M-PER® Mammalian Protein Extraction Reagent (Thermo Scientific) according to the manufacturer's instructions. N-Ethylmaleimide was added at a final concentration of 10 μM during lysis. Protein quantification was performed using the Bradford Protein Assay. To perform western blot analysis, 30 μg of protein were separated by SDS/PAGE in a NuPAGE™ 4–12% Bis-Tris gel (NP0323BOX, Invitrogen) with NuPAGE™ MOPS SDS running buffer (NP0001, Invitrogen).

COS-7 cells were maintained at 37 °C in Dulbecco's Eagle's medium (Sigma-Aldrich, BE12-604F) supplemented with 10% (v/v) of fetal bovine serum (631106, Clontech) and 1% (v/v) penicillin/streptomycin (Invitrogen, 15140-122). COS-7 cells were cultured at 70% confluency and co-transfected with 16 μg of DNA per 10 cm-Petri dish, in a ratio of 1:3. Lipotransfectin reagent (Niborlab) was used according to the manufacturer's instructions. Green Fluorescent Protein expression construct was used as a positive control for transfection. 48 h after transfection, cells were lysed in 1 mL per 10 cm-petri dish of Pierce IP Lysis Buffer (Thermo Scientific, 87787) supplemented with Halt

Protease Inhibitor Cocktail (Thermo Scientific, 78438). Lysates were incubated on ice for 20 min and clarified by centrifugation at 3000 × *g* for 15 min at 4 °C to precipitate proteins. Bradford Protein Assay was used to quantify protein in the spectrophotometer Sinergy HT and analyzed using MultiGauge Software (Fujifilm). To detect the mono-HA-SUMO-2 form, 50 µg of protein were separated by SDS/PAGE in a 12% acrylamide gel.

Western blot analysis

SDS/PAGE, proteins were transferred for 2 h on to PVDF membranes (Millipore), which were blocked with 5% (v/v) non-fat milk in TBS-T [TBS containing 0.1% (v/v) Tween20] for 1 h. Membranes were incubated overnight at 4 °C with the primary antibody (see below) in TBS-T containing 5% (v/v) non-fat milk, washed three times with TBS-T, and incubated for a further 1 h in TBS-T containing 5% (v/v) non-fat milk containing the appropriate secondary antibody. After three washes with TBS-T, membranes were processed with Immobilon® Forte Western Blotting HRP Substrate (Merck Millipore, WBLUF0100) in Li-Cor Odyssey XF imager. Primary antibodies used in Western blotting were anti-HA tag antibody—ChIP Grade (Abcam, ab9110, 1:2000) and anti-alpha Tubulin antibody [DM1A] (Abcam, ab7291, 1:1000), anti-SUMO1 (C-terminal) (S5446, Sigma-Aldrich 1:2000), anti-SUMO2 (S9571, Sigma-Aldrich 1:2000), HRP-conjugated Mouse Anti-Rabbit antibody (light chain-specific) (Cell Signaling Technology, 93702, 1:1000), polyclonal Rabbit anti-mouse immunoglobulin HRP (Dako, P0260, 1:5000).

SUMO-AMC hydrolysis assays

SENP5 wild type and mutants were incubated with SUMO1-AMC (BML-UW0040-0050, ENZO Life Sciences) and SUMO2-AMC (BML-UW0045-0025, ENZO Life Sciences) at 37 °C and fluorescence emission was measured using a Jasco FP-8200 spectrofluorometer at 345 nm excitation and 445 nm emission wavelengths. All measurements were carried out with 50 nM SENP5 and 0.1 µM Ub-AMC in 250 mM NaCl, 20 mM Tris-HCl pH 8, 4 mM DTT buffer.

SUMO-Rhodamine Morpholine hydrolysis assays

The wild-type SENP5 catalytic domain was incubated with labeled SUMO substrates, including WTSUMO1, E67DSUMO1, WTSUMO2, and D63ESUMO2, conjugated to SUMO-Rhodamine Morpholine (prepared in Monique Mulder's lab). Reactions were carried out at 37 °C, and fluorescence emission was measured using a Jasco FP-8200 spectrofluorometer, with excitation at 485 nm and emission at 520 nm. For all measurements, 50 nM SENP5 and 0.5 µM SUMO-Rho were used in a buffer consisting of 250 mM NaCl, 20 mM Tris-HCl (pH 8.0), and 4 mM DTT.

For RANGAP1-SUMO competition assays, the methodology was similar, except that WTSUMO2 was labeled with Rhodamine 110 (purchased from South Bay Bio LLC, SBB-PS0029), with excitation at 485 nm and emission at 535 nm. Increasing concentrations of unlabeled NΔ419RANGAP1-SUMO1, NΔ419RANGAP1-SUMO1E67D, NΔ419RANGAP1-SUMO2, or NΔ419RANGAP1-SUMO2D63E were added to the reaction mixture. An increase in fluorescence signal indicates proteolytic hydrolysis of the amide bond between the C-terminal diGly motif and the rhodamine compound. Conversely, the fluorescence emission rate should decrease in the presence of competitive substrates. The initial $SENP5_{CD}$ activity (initial velocity of fluorescence emission, slope) was set to 100% in the absence of competitive substrates, and the remaining $SENP5_{CD}$ activity (%) was measured with increasing concentrations of the competitive substrates.

In vitro de-SUMOyation assays

$SENP5_{CD}$ protease activity was determined by incubating NΔ419RanGAP1-SUMO1 WT/E67D, NΔ419RanGAP1-SUMO2WT/D63E (1 µM), preSUMO1WT/E67D, preSUMO2WT/D63E (2 µM) or diSUMO2 (1 µM) with 5 nM or 150 nM of SENP5 *wild type* and mutants at 37 °C in a buffer containing 20 mM Tris-HCl (pH 8.0), 250 mM NaCl, and 2 mM DTT. Reactions were stopped with SDS-BME loading buffer and gel electrophoresis (SDS-PAGE) was performed. Gels were stained by SYPRO (Bio-Rad), and proteins were detected and quantified using a Gel-Doc machine with associated integration software (ImageLab; Bio-Rad). The fraction of analyzed bands was plotted as error bar graphs with standard deviations representing the mean ± SEM.

Labeling of endogenous SENP3 in cell lysates

HEK293T cells were harvested in lysis buffer (150 mM NaCl, 50 mM Tris pH 7.5, 0.5% Triton-X100, Protease inhibitor cocktail (Roche, 11873580001)), and collected after sonication (30 s on/off, 5 cycles, 4 °C) and centrifugation (14000 rpm, 4 °C, 10 min). Lysate (40 µL) was incubated with Rho/Bio-SUMO PA probe (40 µL, 1 µM final concentration) for 5 min at 37 °C. Reactions were stopped by the addition of LDS sample buffer containing 10% BME, followed by boiling for 10 min. Samples were resolved by SDS-PAGE, followed by in-gel fluorescence scanning and transfer to nitrocellulose membranes. Membranes were blocked in 5% milk in PBS-T followed by 1 h incubation at room temperature of primary antibody: rabbit anti-SENP3 (1:1000 dilution; Cell Signalling Technology; 5591) and mouse anti-β-actin (1:10000 dilution; Santa Cruz Biotechnology.; sc-47778). This was followed by 1 h incubation at room temperature of fluorescently labelled secondary antibody: anti-rabbit-800 (1:20000 dilution; LiCOR; 926-68021) and anti-mouse-800 (1:20000 dilution; LiCOR; 926-68020). Labelled SENP3 was visualized on a LICOR Odyssey system v3.0.

Data availability

Structures reported here have been deposited in the Protein Data Bank under accession codes 9GNN, 9GNV, and 9GNX. Other Protein Data Bank accession codes used in this study: 2IO0 (SENP2-SUMO2) and 7R2E (SENP7-SUMO2). All other data supporting the findings of this study are available within the article and its supplementary information files. Source data are provided with this paper.

References

1. Varejão, N. et al. Molecular mechanisms in SUMO conjugation. *Biochem. Soc. Trans.* **48**, 123–135 (2020).
2. Bhachoo, J. S. & Garvin, A. J. SUMO and the DNA damage response. *Biochem. Soc. Trans.* **52**, 773–792 (2024).
3. Vertegaal, A. C. O. Signalling mechanisms and cellular functions of SUMO. *Nat. Rev. Mol. Cell Biol.* **23**, 715–731 (2022).
4. Wu, W. & Huang, C. SUMOylation and DeSUMOylation: prospective therapeutic targets in cancer. *Life Sci.* **332**, 122085 (2023).
5. Lascorz, J. et al. SUMO-SIM interactions: from structure to biological functions. *Semin Cell Dev. Biol.* **132**, 193–202 (2022).
6. Chang, H.-M. & Yeh, E. T. H. SUMO: from bench to bedside. *Physiol. Rev.* **100**, 1599–1619 (2020).
7. Yau, T.-Y. et al. SUMO interacting motifs: structure and function. *Cells* **10**, 2825 (2021).
8. Claessens, L. A. & Vertegaal, A. C. O. SUMO proteases: from cellular functions to disease. *Trends Cell Biol.* https://doi.org/10.1016/j.tcb.2024.01.002 (2024).
9. Kunz, K. et al. SUMO-specific proteases and isopeptidases of the SENP family at a glance. *J. Cell Sci.* **131**, jcs211904 (2018).
10. Hickey, C. M. et al. Function and regulation of SUMO proteases. *Nat. Rev. Mol. Cell Biol.* **13**, 755–766 (2012).
11. Yeh, E. T. H. SUMOylation and De-SUMOylation: Wrestling with Life's Processes *. *J. Biol. Chem.* **284**, 8223–8227 (2009).
12. Bouchard, D. et al. SUMO paralogue-specific functions revealed through systematic analysis of human knockout cell lines and gene expression data. *Mol. Biol. Cell* **32**, 1849–1866 (2021).

13. Wang, W. & Matunis, M. J. Paralogue-specific roles of SUMO1 and SUMO2/3 in protein quality control and associated diseases. *Cells* **13**, 8 (2024).
14. Owerbach, D. et al. A proline-90 residue unique to SUMO-4 prevents maturation and sumoylation. *Biochem. Biophys. Res. Commun.* **337**, 517–520 (2005).
15. Drag, M. & Salvesen, G. S. DeSUMOylating enzymes-SENPs. *IUBMB Life* **60**, 734–742 (2008).
16. Nayak, A. & Müller, S. SUMO-specific proteases/isopeptidases: SENPs and beyond. *Genome Biol.* **15**, 422 (2014).
17. Mukhopadhyay, D. & Dasso, M. Modification in reverse: the SUMO proteases. *Trends Biochem Sci.* **32**, 286–295 (2007).
18. Barrett, A. J. & Rawlings, N. D. Evolutionary lines of cysteine peptidases. *Biol. Chem.* **382**, 727–733 (2001).
19. Mossessova, E. & Lima, C. D. Ulp1-SUMO crystal structure and genetic analysis reveal conserved interactions and a regulatory element essential for cell growth in yeast. *Mol. Cell* **5**, 865–876 (2000).
20. Li, S. J. & Hochstrasser, M. A new protease required for cell-cycle progression in yeast. *Nature* **398**, 246–251 (1999).
21. Suh, H.-Y. et al. Crystal structure of DeSI-1, a novel deSUMOylase belonging to a putative isopeptidase superfamily. *Proteins* **80**, 2099–2104 (2012).
22. Li, Y. et al. Structural basis for the SUMO protease activity of the atypical ubiquitin-specific protease USPL1. *Nat. Commun.* **13**, 1819 (2022).
23. Schulz, S. et al. Ubiquitin-specific protease-like 1 (USPL1) is a SUMO isopeptidase with essential, non-catalytic functions. *EMBO Rep.* **13**, 930–938 (2012).
24. Wagner, K. et al. The SUMO isopeptidase SENP6 functions as a rheostat of chromatin residency in genome maintenance and chromosome dynamics. *Cell Rep.* **29**, 480–494.e5 (2019).
25. Lima, C. D. & Reverter, D. Structure of the human SENP7 catalytic domain and poly-SUMO deconjugation activities for SENP6 and SENP7. *J. Biol. Chem.* **283**, 32045–32055 (2008).
26. Hay, R. T. SUMO-specific proteases: a twist in the tail. *Trends Cell Biol.* **17**, 370–376 (2007).
27. Hang, J. & Dasso, M. Association of the Human SUMO-1 Protease SENP2 with the Nuclear Pore *. *J. Biol. Chem.* **277**, 19961–19966 (2002).
28. Reverter, D. & Lima, C. D. A basis for SUMO protease specificity provided by analysis of human Senp2 and a Senp2-SUMO complex. *Structure* **12**, 1519–1531 (2004).
29. Reverter, D. & Lima, C. D. Structural basis for SENP2 protease interactions with SUMO precursors and conjugated substrates. *Nat. Struct. Mol. Biol.* **13**, 1060–1068 (2006).
30. Shen, L. et al. SUMO protease SENP1 induces isomerization of the scissile peptide bond. *Nat. Struct. Mol. Biol.* **13**, 1069–1077 (2006).
31. Liu, W. et al. Lactate regulates cell cycle by remodelling the anaphase promoting complex. *Nature* **616**, 790–797 (2023).
32. Heo, K.-S. et al. Disturbed flow-activated p90RSK kinase accelerates atherosclerosis by inhibiting SENP2 function. *J. Clin. Invest.* **125**, 1299–1310 (2015).
33. Raman, N. et al. mTOR signaling regulates nucleolar targeting of the SUMO-specific isopeptidase SENP3. *Mol. Cell Biol.* **34**, 4474–4484 (2014).
34. Li, Y.-Y. et al. TCR-induced tyrosine phosphorylation at Tyr270 of SUMO protease SENP1 by Lck modulates SENP1 enzyme activity and specificity. *Front Cell Dev. Biol.* **9**, 789348 (2022).
35. Jiang, M. et al. SUMO-specific protease 2 in Mdm2-mediated regulation of p53. *Cell Death Differ.* **18**, 1005–1015 (2011).
36. Cubeñas-Potts, C. et al. SENP1 and SENP2 affect spatial and temporal control of sumoylation in mitosis. *Mol. Biol. Cell* **24**, 3483–3495 (2013).
37. Goeres, J. et al. The SUMO-specific isopeptidase SENP2 associates dynamically with nuclear pore complexes through interactions with karyopherins and the Nup107-160 nucleoporin subcomplex. *MBoC* **22**, 4868–4882 (2011).
38. Gong, L. & Yeh, E. T. H. Characterization of a family of nucleolar SUMO-specific proteases with preference for SUMO-2 or SUMO-3. *J. Biol. Chem.* **281**, 15869–15877 (2006).
39. Haindl, M. et al. The nucleolar SUMO-specific protease SENP3 reverses SUMO modification of nucleophosmin and is required for rRNA processing. *EMBO Rep.* **9**, 273–279 (2008).
40. Yun, C. et al. Nucleolar protein B23/nucleophosmin regulates the vertebrate SUMO pathway through SENP3 and SENP5 proteases. *J. Cell Biol.* **183**, 589–595 (2008).
41. Zunino, R. et al. The SUMO protease SENP5 is required to maintain mitochondrial morphology and function. *J. Cell Sci.* **120**, 1178–1188 (2007).
42. Zunino, R. et al. Translocation of SenP5 from the nucleoli to the mitochondria modulates DRP1-dependent fission during mitosis. *J. Biol. Chem.* **284**, 17783–17795 (2009).
43. Maison, C. et al. The SUMO protease SENP7 is a critical component to ensure HP1 enrichment at pericentric heterochromatin. *Nat. Struct. Mol. Biol.* **19**, 458–460 (2012).
44. Bawa-Khalfe, T. et al. Differential expression of SUMO-specific protease 7 variants regulates epithelial-mesenchymal transition. *Proc. Natl. Acad. Sci. USA* **109**, 17466–17471 (2012).
45. Romeo, K. et al. The SENP7 SUMO-protease presents a module of Two HP1 interaction motifs that Locks HP1 protein at pericentric heterochromatin. *Cell Rep.* **10**, 771–782 (2015).
46. Yamada, S. et al. Drp1 SUMO/deSUMOylation by Senp5 isoforms influences ER tubulation and mitochondrial dynamics to regulate brain development. *iScience* **24**, 103484 (2021).
47. Di Bacco, A. & Gill, G. SUMO-specific proteases and the cell cycle: An essential role for SENP5 in cell proliferation. *Cell Cycle* **5**, 2310–2313 (2006).
48. Kim, E. Y. et al. SENP5, a SUMO isopeptidase, induces apoptosis and cardiomyopathy. *J. Mol. Cell Cardiol.* **78**, 154–164 (2015).
49. Panse, V. G. et al. Formation and nuclear export of preribosomes are functionally linked to the small-ubiquitin-related modifier pathway. *Traffic* **7**, 1311–1321 (2006).
50. Dönig, J. et al. Characterization of nucleolar SUMO isopeptidases unveils a general p53-independent checkpoint of impaired ribosome biogenesis. *Nat. Commun.* **14**, 8121 (2023).
51. Yu, B. et al. SUMO proteases SENP3 and SENP5 spatiotemporally regulate the kinase activity of Aurora A. *J. Cell Sci.* **134**, jcs249771 (2021).
52. Li, Y. et al. Structural basis for the SUMO2 isoform specificity of SENP7. *J. Mol. Biol.* **434**, 167875 (2022).
53. Alegre, K. O. & Reverter, D. Swapping small ubiquitin-like modifier (SUMO) isoform specificity of SUMO proteases SENP6 and SENP7. *J. Biol. Chem.* **286**, 36142–36151 (2011).
54. Alegre, K. O. & Reverter, D. Structural insights into the SENP6 Loop1 structure in complex with SUMO2. *Protein Sci.* **23**, 433–441 (2014).
55. Di Bacco, A. et al. The SUMO-specific protease SENP5 is required for cell division. *Mol. Cell Biol.* **26**, 4489–4498 (2006).
56. Mulder, M. P. C. et al. Total chemical synthesis of SUMO and SUMO-based probes for profiling the activity of SUMO-specific proteases. *Angew. Chem. Int. Ed.* **57**, 8958–8962 (2018).
57. Sommer, S. et al. Covalent inhibition of SUMO and ubiquitin-specific cysteine proteases by an in situ thiol–alkyne addition. *Bioorg. Med. Chem.* **21**, 2511–2517 (2013).
58. Hemelaar, J. et al. Chemistry-based functional proteomics: mechanism-based activity-profiling tools for ubiquitin and ubiquitin-like specific proteases. *J. Proteome Res.* **3**, 268–276 (2004).
59. Krissinel, E. & Henrick, K. Inference of macromolecular assemblies from crystalline state. *J. Mol. Biol.* **372**, 774–797 (2007).

60. Reverter, D. et al. Structure of a complex between Nedd8 and the Ulp/Senp protease family member Den1. *J. Mol. Biol.* **345**, 141–151 (2005).
61. Gan-Erdene, T. et al. Identification and characterization of DEN1, a deneddylase of the ULP family *. *J. Biol. Chem.* **278**, 28892–28900 (2003).
62. Garvin, A. J. et al. The deSUMOylase SENP7 promotes chromatin relaxation for homologous recombination DNA repair. *EMBO Rep.* **14**, 975–983 (2013).
63. Claessens, L. A. et al. SENP6 regulates localization and nuclear condensation of DNA damage response proteins by group deSUMOylation. *Nat. Commun.* **14**, 5893 (2023).
64. Liebelt, F. et al. The poly-SUMO2/3 protease SENP6 enables assembly of the constitutive centromere-associated network by group deSUMOylation. *Nat. Commun.* **10**, 3987 (2019).
65. Albuquerque et al. Binding to small ubiquitin-like modifier and the nucleolar protein Csm1 regulates substrate specificity of the Ulp2 protease. *J. Biol. Chem.* **293**, 12105–12119 (2018).
66. Roberts, C. G. et al. Ubiquitin-targeted bacterial effectors: rule breakers of the ubiquitin system. *EMBO J.* **42**, e114318 (2023).
67. Pruneda, J. N. et al. The molecular basis for ubiquitin and ubiquitin-like specificities in bacterial effector proteases. *Mol. Cell* **63**, 261–276 (2016).
68. Sánchez-Alba, L. et al. Structural diversity of the CE-clan proteases in bacteria to disarm host ubiquitin defenses. *Trends Biochem. Sci.* **49**, 1111–1123 (2024).
69. Lara-Ureña, N. et al. Cancer-associated dysregulation of sumo regulators: proteases and ligases. *Int. J. Mol. Sci.* **23**, 8012 (2022).
70. van den Ent, F. & Löwe, J. RF cloning: a restriction-free method for inserting target genes into plasmids. *J. Biochem Biophys. Methods* **67**, 67–74 (2006).
71. Bachman, J. Chapter Ninteen - Site-directed mutagenesis. In *Methods in Enzymology* Vol. 529 (ed. Lorsch, J.), pp. 241–248, (Academic Press, 2013).
72. Vernier, M. et al. Regulation of E2Fs and senescence by PML nuclear bodies. *Genes Dev.* **25**, 41–50 (2011).
73. Terui, Y. et al. Dual role of sumoylation in the nuclear localization and transcriptional activation of NFAT1. *J. Biol. Chem.* **279**, 28257–28265 (2004).
74. Békés, M. et al. The dynamics and mechanism of SUMO chain deconjugation by SUMO-specific proteases. *J. Biol. Chem.* **286**, 10238–10247 (2011).
75. Kooij, R. et al. Small-molecule activity-based probe for monitoring ubiquitin C-terminal hydrolase L1 (UCHL1) activity in live cells and zebrafish embryos. *J. Am. Chem. Soc.* **142**, 16825–16841 (2020).
76. Juanhuix, J. et al. Developments in optics and performance at BL13-XALOC, the macromolecular crystallography beamline at the Alba Synchrotron. *J. Synchrotron Rad.* **21**, 679–689 (2014).
77. Vonrhein, C. et al. Data processing and analysis with the autoPROC toolbox. *Acta Cryst. D.* **67**, 293–302 (2011).
78. Emsley, P. et al. Features and development of Coot. *Acta Cryst. D.* **66**, 486–501 (2010).
79. Adams, P. D. et al. PHENIX: a comprehensive Python-based system for macromolecular structure solution. *Acta Cryst. D.* **66**, 213–221 (2010).

Acknowledgements

This work was supported by the Spanish Ministry of Science and Innovation (MICINN) PID2021–124602OB-I00 to D.R. and by ICREA to D.R., ICREA-Academia-2022, from Generalitat de Catalunya. Y.L. acknowledges her support by the National Natural Science Foundation of China (grant No.32300040). L.S.A. acknowledges her FPI fellowship from the Spanish Government (grant No PRE2019-088509). MPCM acknowledges her support by the Netherlands Organization for Scientific Research (NWO) (VIDI Grant VI. 213.110). D.R. acknowledges support from the Serra Hunter program from Generalitat de Catalunya. X-ray experiments were performed at BL-13 XALOC beamline at ALBA Synchrotron with the collaboration of ALBA staff.

Author contributions

Y.L. and L.S.A. conducted crystallization experiments. Y.L., L.S.A., B.L., H.B.G., and N.V. conducted all in vitro activity assays. L.S.A., A.D.B., and V.A. conducted cultured cell assays. M.D.M. and M.P.C.M. synthesized SUMO chemical probes and conducted cell lysate labeling. D.R., N.V., and L.S.A. contributed to the correction and writing of the manuscript.

Competing interests

The authors declare no competing interests.

Additional information

Supplementary information The online version contains supplementary material available at https://doi.org/10.1038/s41467-025-60029-4.

Correspondence and requests for materials should be addressed to David Reverter.

Peer review information *Nature Communications* thanks the anonymous reviewer(s) for their contribution to the peer review of this work. A peer review file is available.